THE JOURNAL OF PHYSICAL CHEMISTRY B

Article

pubs.acs.org/JPCB

Computational Investigation on the Effect of Alumina Hydration on Lithium Ion Mobility in Poly(ethylene oxide) $LiClO_4$ Electrolytes

Hui Wu, Oneka T. Cummings, and Collin D. Wick*

Louisiana Tech University, Ruston, Louisiana 71270, United States

ABSTRACT: Improving ionic conductivity and lithium ion mobility in polymer electrolytes is important for their practical use for polymer electrolytes. In this study, a combination of molecular dynamics and Monte Carlo simulations were used to bring insight into lithium ion transport in poly(ethylene oxide) $LiClO_4$ polymer electrolytes next to both acidic and basic treated model alumina solid surfaces at 323, 348, and 373 K. The acidic treated system had hydrogens present on its surface, while the basic treated system did not. The results found reduced ion mobility near the surfaces and little change to overall conductivity away from the surface. However, ion diffusion was somewhat enhanced for the acidic treated system at 323 K in comparison with systems without any surface present, despite that close to the surface it was reduced. This was linked to long-ranged structural ordering of ions in the system brought on by strong interactions with the surface, which resulted in oscillations in lithium and ClO_4^- densities that were out of phase, reducing ion binding and enhancing diffusivities.

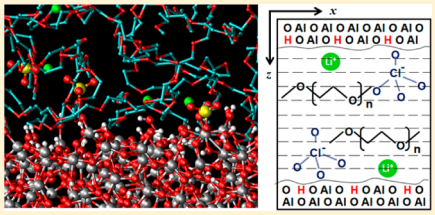

I. INTRODUCTION

Due to the unreliable supply of oil facing our country and the world today, finding ways to make electrical energy more viable is important for our economic security. Battery technology is one of the most promising avenues for a reliable and cost-effective medium to store energy for portable devices and vehicles. In recent decades, rechargeable lithium batteries (RLBs) have become common in consumer electronics for relatively low power applications, while extensive research and development has improved the technology for use on board military equipment, and electric and hybrid vehicles.[1−6] One major component of RLBs is their electrolyte, which needs to have a high level of stability while promoting high mobility or lithium ions. Traditional electrolytes are mostly organic liquids, such as cyclic carbonates, along with lithium salts, such as $LiBF_4$, $LiCF_3SO_3$, $LiPF_6$, LiTFSI, $LiClO_4$, or similar.[7−12] Safety concerns arise due to the corrosive and toxic nature of the liquid electrolytes, which can cause major problems if leakage occurs. Furthermore, at high temperatures and in overcharging situations, carbonate electrolytes can react with the electrodes, creating gases that cause the batteries to break, resulting in fire or explosion.[7,13−16]

To eliminate problems associated with liquid electrolytes, a solid polymer electrolyte (SPE) can be used in place of liquid electrolytes, since they are virtually free of leakage and have a high degree of chemical stability. SPEs also have other advantages, including potential low cost design, flexibility in a wide variety of packaging shapes, good electrochemical stability, enhanced mechanical properties, low flammability, low corrosive properties, and the ability to form good interfacial contacts with electrodes.[5,17,18] The most investigated SPE is poly(ethylene oxide) (PEO) with the addition of lithium salts of the form LiX (X^- = ClO_4^-,[11,19−33] $TFSI^-$,[34−36] $CF_3SO_3^-$,[10,11,37−42] I^-,[11,43,44] and BF_4^-[45]) to allow the conduction of lithium ions, in which the segmental motion of the PEO chains assists in ion motion. The ionic conductivity of SPEs at room temperature is on the order of 10^{-4}−10^{-7} S/cm,[18] while at least 10^{-3} S/cm is required to be commercially viable.[5,6,46,47] The cited reason for this low conductivity is that SPEs become crystalline near room temperature, significantly reducing dynamic movement, and reducing their efficiency.[48] Thus, diverse studies of trying to minimize crystallization and modifying the composites have been pursued to improve ionic conductivity.[17]

One approach to improve the conductance of SPEs is to incorporate plasticizers into the polymer matrix,[24,49,50] such as cyclic carbonates[24,26,41−44] and low molecular weight poly(ethylene glycol).[11] Depending on the amount of plasticizer introduced, the ionic conductivities of the plasticized SPEs can approach commercially viable values, but they have two main weaknesses. Since a large liquid component is added to the polymer, the mechanical properties are weakened with respect to SPEs. Furthermore, the separation of the liquid fraction from the polymer, indicated as syneresis, can be a problem and lead to electrolyte breakdown.[12] There have been strategies developed to improve these, including cross-linking the polymers,[51] and placing low molecular weight polymer into a network of cross-linked fumed silica.[52−54]

Another avenue to improve the ambient temperature ionic conductivity without weakening the mechanical properties of the SPEs is to add nanoparticles such as $LiAlO_2$, SiO_2, Al_2O_3, or TiO_2 in PEO based polymer electrolytes to make nanocomposite polymer electrolytes.[20−22,25−27,29,32,45,55−65] It has been shown that ionic conductivity is enhanced at ambient temperatures due to the nanoparticles decreasing the degree of crystallinity of the PEO−salt system at least temporarily.[2,66]

Received: August 6, 2012
Revised: November 30, 2012
Published: December 17, 2012

The source of the conductivity increase can be attributed to interactions between the polymer and lithium salts and the surface of the nanoparticles, which is enhanced due to the large amount of nanoparticle surface area present.[55,59] Besides improvements in ionic conductivity, nanocomposite PEO-based electrolytes have also shown improved mechanical and thermal stability, and a consistent enhanced lithium transference, which is a measure of the amount of conductivity due to lithium ion motion, has been found both below and above the PEO crystallization temperature.[57,58]

Investigations of the role of these nanoparticles on the conductivity of LiX salts in PEO have focused on a variety of factors but are often found to be related to the nature of the interactions between PEO−LiX and the nanoparticle surface.[2,67−69] One such study found that different conductivities and lithium transference were found to depend on if the alumina nanoparticles were treated with acid or base.[59] The acidic treated system showed both higher conductivities and lithium transference than the basic treated system, which was attributed to OH groups binding with the PEO chains, along with the anion ($CF_3SO_3^-$). On the other hand, the basic system had alumina with few hydrogens present, so the oxygens on the alumina surface were conjectured to interact primarily with lithium, slowing their movement.[59]

To truly develop an understanding of how nanoparticles influence ionic conductivity in polymer electrolytes, a molecular level picture needs to be developed that can be verified with experiment. Molecular simulations can be used as a complement to experiments due to their ability to provide detailed molecular level information related to the ion transport mechanism next to the solid interface. Furthermore, diffusivities and ionic conductivities can be calculated to provide a direct comparison with experiments. The conduction mechanism for lithium in PEO near a nanoparticle surface has been investigated by computational methods.[70−76] PEO/LiX with X = Cl^-, Br^-, I^-, and BF_4^- was investigated with an Al_2O_3 nanoparticle present.[73−75] In these studies, it was found that lithium ion mobility was increased by introducing a nanoparticle in PEO, and that the enhancement of lithium mobility was related to LiX pairing and clustering, which occurred away from the nanoparticle surface.[73−75] It should be noted that these studies were carried out for a rather short period of time, around 1 ns, which is not long enough to ensure equilibration of the systems, but brought significant initial insight into these systems.[73−75] Molecular dynamics simulations of PEO sandwiched between two TiO_2 surfaces were carried out.[72] These studies found that TiO_2 significantly enhanced the PEO density up to 15 Å away from the surface, and that PEO dynamics were significantly reduced in this region.[72] Further work by the same group investigated PEO/$LiBF_4$ near a TiO_2 nanoparticle and also near a nanoparticle with soft repulsive (SR) interactions with PEO.[70] It was reported that $LiBF_4$ concentration was lower near the TiO_2 nanoparticle due to strong PEO−TiO_2 interactions but that the ion concentration near the SR nanoparticle was enhanced with respect to regions far away. This resulted in enhanced ion mobility near the SR nanoparticle resulting in the SR nanoparticle increasing the overall ion diffusion. On the other hand, TiO_2 lowered ion diffusion near its surface but had little effect more than 15 Å away from the nanoparticle.

Investigations of PEO oligomers near silica surfaces found similar results as near TiO_2 with PEO densely packing around the surface.[71] Additionally, poly(dimethylsiloxane) (PDMS) polymers in contact with bare silica showed similar behavior, but when the silica surface was modified with trimethylsiloxy groups, the PDMS density was found to be reduced with respect to the bare silica surface.[77] In this study, the degree of silica hydroxylation was investigated also, finding that greater hydroxylation reduced the PDMS density near the silica surface, increasing its diffusion. However, PDMS diffusion at hydroxylated silica surfaces was still significantly slower than in the region far away from the silica surface.[77]

As described previously, the treatment of the solid surface influences ionic conductivity and lithium transference.[59] While previous computational studies have focused on investigating the role of surface−polymer interactions on lithium mobility, none of these have specifically investigated how acidic versus basic treated surfaces influence it. This paper describes a study in which the influence of alumina, with and without hydrogen atoms present (to represent acidic or basic treated alumina), influences lithium ion mobility and polymer structure in PEO−$LiClO_4$ polymer electrolytes. Computational methods are used to bring molecular level insight into the mechanism of lithium ion transport and how it is influenced by the presence of alumina, including its surface composition.

II. MOLECULAR MODELS

The transferable potentials for phase equilibria united-atom (TraPPE-UA) force field was used for PEO,[78−80] which has been shown to be good for reproducing the structural properties of high molecular weight PEO over a wide range of temperatures and pressures.[78,81] The all-atom ClO_4^- force field, developed by M. Baaden et al.,[82] was used, and the Dreiding force field was utilized for aluminum.[83] The alumina intramolecular interactions were taken from G. Gutierrez and B. Johansson, which is a fixed charge model with exponential-6 interactions.[84]

To develop interaction parameters between the alumina and the polymer/lithium/ClO_4^-, we carried out DFT B3LYP calculations with the aug-cc-pvdz basis set to parametrize them. Two different alumina clusters were modeled, one $Al_8O_{14}H_4$ cluster, which represented the acidic system (four Al_2O_3 groups with two water molecules), and one $Al_8O_{13}H_2$ cluster, which represented the basic system. Figure 1 gives a snapshot of the different clusters that were used to parametrize the interaction energies. The alumina charges were taken from the work of G. Gutierrez and B. Johansson.[84] We parametrized the Lennard-Jones (LJ) interactions to describe the interaction energies and distances from the DFT calculations. The acidic cluster was used for most of the parametrizations, since dimethyl ether (DME) and ClO_4^- do not have strong interactions with the alumina oxygen, and only the lithium ion does. The counterpoise corrected minimum energies from the DFT calculations, along with the distances, are given in Table 1. The LJ interactions between alumina oxygens were parametrized to give the correct binding with lithium and DME. Oxygens bound with hydrogen atoms were parametrized differently than those not bound with hydrogens.

Table 2 gives the LJ parameters for the different alumina oxygen atoms (those bound with a hydrogen, denoted O(H), and those not bound to hydrogen denoted O(Al)). For lithium and DME, the minimum energy distances agreed well between the model and the *ab initio* results, while the binding energies between lithium and the clusters were somewhat underpredicted with respect to *ab* initio calculations. This is consistent with how lithium binds with the DME oxygen

dx.doi.org/10.1021/jp307794r | J. Phys. Chem. B 2012, 116, 14922−14932

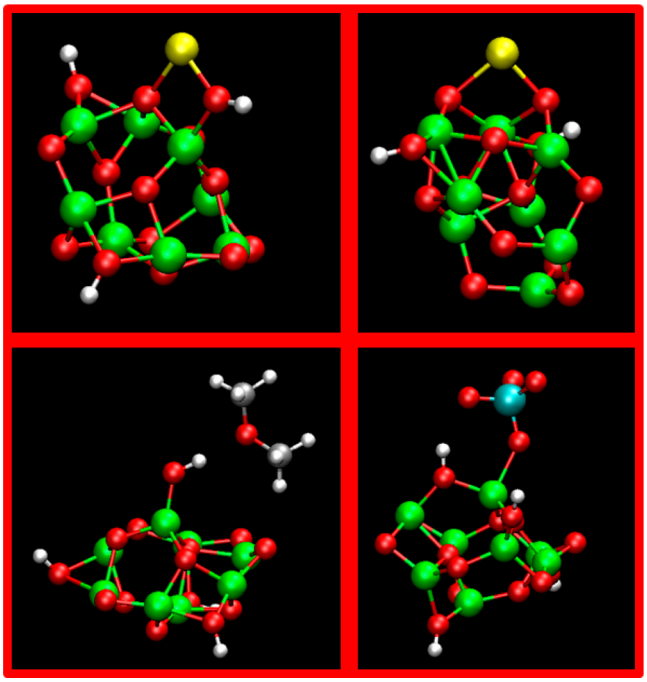

Figure 1. Snapshot of the clusters used to calculate the binding energy of different species with the acidic and basic oxygens. The top left panel is lithium with the acidic cluster, the top right is lithium with the basic cluster, the bottom left is DME with the acidic cluster, and the bottom right is ClO_4^- with the acidic cluster.

Table 1. Comparison of Our Model and *Ab Initio* Results for Interactions between Different Species Investigated with Energy Units of kcal/mol

system	$r_{ab\ initio}$ (Å)	$U_{ab\ initio}$	r_{model}	U_{model}
Li^+–O(H)	1.81	−64.1	1.80	−58.2
Li^+–O(Al)	1.81	−59.2	1.80	−52.5
O_{DME}–O(H)	2.83	−4.53	2.83	−4.32
O(ClO_4)–O(H)	2.76	−50.3	2.83	−37.4
O(ClO_4)–Al	1.93	−50.3	2.00	−37.4
Li^+–O(DME)[a]	1.82	−38.0	1.81	−30.9

[a]Taken from MP2 calculations from refs 86 and 111.

Table 2. LJ Parameters for Some of the Atoms Modeled

	q (e)	σ (Å)	ε (kcal/mol)
Li	+1.000	1.40	0.40
O(H)	−0.945	3.48	0.10
O(Al only)	−0.945	2.95	0.10
H	+0.4725	0.00	0.00

(parametrized in previous work),[81] in which the binding energy is somewhat underpredicted. Polarizable models often do a better job of predicting the correct binding between lithium ions and oxygens,[85,86] but the addition of polarizable interactions increases the computational time significantly, and very long simulations are required to get reasonable results for the systems and conditions being investigated. Furthermore, as described later, Monte Carlo (MC) simulations are used for the system equilibration, and MC simulations are generally very inefficient in their handling of polarizable interactions. The work is also qualitative in nature to determine the influence of acidic and basic treated alumina on ionic conductivity and lithium transference in PEO–$LiClO_4$. Because of this, non-polarizable interactions are used, but it should be noted that polarizable interactions are the best approach if a quantitatively accurate description of these properties is sought.[87−91]

There were some challenges in the DFT calculations with ClO_4^- and alumina, as the ClO_4^- ion dissociated in some of the minimizations with the cluster. The final cluster arrived at is shown in Figure 1, and it still appears that there may be a weak bond formed between the ClO_4^- oxygen and alumina atom. Because of this, the *ab initio* results showed somewhat stronger binding energies for the ClO_4^-–alumina cluster than the model, which is classical and does not incorporate chemical binding. It should be noted that one of the potential reasons for higher lithium transference with the addition of alumina may be chemical binding between the alumina surfaces and ClO_4^-. The final results showed a somewhat smaller minimum energy distance (by around 0.07 Å) for the *ab initio* cluster in comparison with the model cluster and stronger binding from the *ab initio* results.

III. SIMULATION DETAILS

III.A. System Parameters. There were three different types of systems investigated. All three included 4 PEO chains with a number averaged molecular weight of 10 000 g/mol, and 60 $LiClO_4$ ion pairs to give EO:Li = 15:1. Many of the experimental measurements that are being compared have a number averaged molecular weight of 2×10^6 g/mol, but the dependence of molecular weight on ionic conductivity was found to level off at around 10 000 g/mol.[92] For one of the systems investigated, denoted the BULK system, the described molecules were placed in a cubic box. For the other two systems, the box was elongated in the z-direction to a dimension of approximately 120 Å, and x, y dimensions of 28 Å. Both of these systems with an elongated box then had a solid slab of aluminum oxide placed in it (see Figure 2) with an

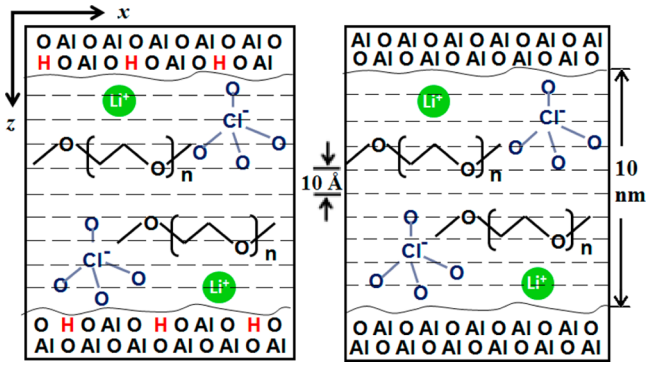

Figure 2. Schematic of the ACID system (left) and the BASE system (right). Dashed lines are spaced in 10 Å increments.

approximate thickness of 20 Å in the z-dimension. Two types of solid slabs were simulated, one with hydrogens present to represent the acidic system (ACID) and one without any hydrogens present to represent the basic system (BASE). All simulations had a potential truncation of 12 Å for non-electrostatic nonbonded interactions (i.e., LJ for liquid–alumina and liquid–liquid interactions and exponential-6 for intramolecular alumina interactions) with analytic tail corrections. The handling of electrostatic interactions depended on the type of simulation. Monte Carlo simulations utilized the regular Ewald summation technique,[93] while molecular

dx.doi.org/10.1021/jp307794r | J. Phys. Chem. B 2012, 116, 14922−14932

dynamics simulations utilized the particle mesh Ewald summation technique.[94]

The distance between the solid slabs, 100 Å, is similar to that of nanoporous alumina membranes, which can be fabricated with an average pore size of 10 nm, and have been used as separators for liquid electrolytes.[95] There is an obvious difference between a solid slab and a cylindrical pore or a nanoparticle surface, but the qualitative effect of alumina on ionic conductivity and lithium transference should be similar between these systems.

III.B. Equilibration of the Systems. The amorphous alumina slab was created by placing 900 Al and 1350 O atoms in a region with a z-dimension of 20 Å and x, y dimensions of 28 Å. The solid was periodic in the x and y dimensions forming two surfaces normal to the z-axis. Molecular dynamics (MD) simulations were then carried out with a 0.5 fs time step to anneal the system at 2000 K for 100 ps in the NVT ensemble, followed by 100 ps of cooling at 400 K. All MD simulations utilized the Berendsen thermostat to control the temperature, and the pressure when NPT simulations were performed.[96] Next, the solid slab was further equilibrated for 100 ps in the NVT ensemble at temperatures of 323, 348, and 373 K, where each temperature represented a different system. This represented the BASE system, since it had no hydrogens present. For the ACID system, 50 water molecules were placed randomly on each surface of the solid slab, followed by a short 10 ps equilibration at 400 K in the NVT ensemble, followed by 100 ps of annealing at 2000 K and 100 ps of cooling at 400 K all in the NVT ensemble. This was followed by 100 ps in the NVT ensemble at 323, 348, and 373 K.

As stated, three PEO−$LiClO_4$ systems were simulated: one with no solid present (BULK system), the ACID system, and the BASE system. All had equal numbers of PEO chains, number averaged PEO molecular weight (10 000 g/mol), and $LiClO_4$ ion pairs. The reason we report the number averaged molecular weight is that it was allowed to vary in the MC simulations between 7500 and 12 500 g/mol, which was treated in the semi-grand-canonical ensemble as has been done previously.[97] These species (PEO and $LiClO_4$) were initially equilibrated with MC simulations. The MC simulations utilized multiple moves designed to efficiently equilibrate polymer structure, which included polymer reptation moves, configurational-bias,[98−101] self-adapting fixed-end-point configurational-bias,[102] end-bridging,[97] and double-bridging Monte Carlo moves.[103] These are in addition to the regular MC translational, rotational, and volume moves.[93] The ratio of their use and more specifics are given in previous work.[81] For the BULK system, an initial temperature of 500 K was utilized to speed up the equilibration of the system in the NVT ensemble (i.e., no volume moves), in which 100 000 MC cycles (where each cycle includes the number of moves equal to the number of molecules present) were performed. Following this, 100 000 MC cycles of simulations were carried out in the NPT ensemble at 1.0 atm to equilibrate the system at one of three temperatures, 323, 348, and 373 K. These simulations were then followed by 100 ns of equilibration in the NPT ensemble via MD simulations at the described temperatures with a time step of 1 fs.

Calculations for the ACID and BASE systems started from the same initial configuration in which the number of PEO chains and $LiClO_4$ molecules were placed in the orthorhombic box with dimensions described in the previous section. A repulsive potential of the form A/z^{12} with A = 100 kcal/mol on each side of a slab of thickness 2 nm was incorporated into the simulations, where the alumina slab was to be added later. An initial equilibration of 100 000 MC cycles at 500 K in the NVT ensemble was carried out for this system. During this high temperature equilibration period, the system was checked to ensure that the PEO and $LiClO_4$ density in the system were fairly uniform. Next, the annealed alumina slabs were placed in this repulsive region, creating both the ACID and BASE systems, which included the respective alumina slabs, PEO, and $LiClO_4$. The repulsive potential was then removed, and an additional 100 000 MC cycles at 500 K were carried out in the NVT ensemble. After this, another 100 000 MC cycles were carried out, saving the coordinates of the system in 20 000 MC cycle increments to save a total of six independent coordinate sets for both the ACID and BASE systems. During this initial equilibration period, no movement of the alumina atoms was allowed. Next, 100 000 MC cycles were performed on each system in the NPT ensemble at 1 atm and the three respective temperatures, 323, 348, and 373 K. Four independent simulations were carried out for each system type (ACID and BASE) at 323 K, and one simulation was carried out for each type at 348 and 373 K. The reason for having four at 323 K is because the statistics are the most challenging to collect at those temperatures, and most experimentally meaningful differences due to the inclusion of alumina occur there.[31] MD simulations in the NPT ensemble were then spawned from these, and 100 ns of equilibration at 1 atm and their respective temperatures were carried out.

III.C. Calculation of Properties. After equilibration, all simulations were carried out for a minimum of 200 ns to calculate properties with more at the 323 K temperature. The principal process of ion transport in polymer electrolytes is of primary importance to assess their usage.[104−106] The ionic conductivity (λ) can be calculated utilizing the Einstein relation

$$\lambda = \lim_{\tau\to\infty} \frac{e^2}{2dtVk_BT} \sum_{i=1}^{N}\sum_{j=1}^{N} z_i z_j \langle [\mathbf{r}_i(\tau) - \mathbf{r}_i(0)] \cdot [\mathbf{r}_j(\tau) - \mathbf{r}_j(0)] \rangle \quad (1)$$

where the summation is over all ionic species (N) and $\mathbf{r}_i(\tau)$ represents the vector position of species i at time τ. Also, z_i represents the ionic charges, V the volume, e the electron charge, k_B the Boltzmann constant, d the dimensions of the system, and T the temperature. The brackets denote the ensemble average. The diffusion coefficient for species i can be calculated with the following relation

$$D_i = \lim_{\tau\to\infty} \frac{\langle [\mathbf{r}_i(\tau) - \mathbf{r}_i(0)]^2 \rangle}{2d\tau} \quad (2)$$

where the symbols are the same as represented in eq 1. For the BULK system, eqs 1 and 2 can be used with d = 3 to calculate the ionic conductivity and diffusion coefficient. With a solid surface present, a somewhat different approach is needed, as diffusion has a barrier perpendicular to the surface. One can calculate diffusion and conductivity for the region parallel to an interface, or along the xy dimensions in Figure 2. The vectors in eqs 1 and 2 will only include the x and y components, and d = 2. For the simulations in the BULK system, along with the calculations with the alumina surfaces, the results were from 200 ns for 348 and 373 K and 400 ns at 323 K, except where noted otherwise. Additionally, the diffusion coefficient can be split up into different regions, which were chosen to be 10 Å

slabs, as shown in Figure 2. A previously developed method[107,108] was used to calculate the described values in the individual regions using the following methodology. First, the survival probability, $P(\tau)$, for each ion to stay within a certain region ($\mathbf{R}_k$) for the time interval (0, τ) was calculated

$$P_i(\tau) = \frac{N_i(0, \tau)}{N_i(0)} \tag{3}$$

where $N_i(0)$ indicates the number of species i that *originate* in a certain region at the beginning of the time interval and $N_i(0, \tau)$ indicates the number of species i that stay within the region for the *entirety* of the time interval. It should be emphasized that, if the species leaves the region for even one time step, it is not counted. Next, the mean square displacements of the ion i that stay within a specified region $\mathbf{R}_k$ for the entirety of the time interval can be determined

$$\langle \Delta \mathbf{r}(\tau)^2 \rangle_{\mathbf{R}_k} = \frac{1}{N_i(0)} \sum_{i \in \mathbf{R}_k} [\mathbf{r}_i(\tau) - \mathbf{r}_i(0)]^2 \tag{4}$$

Finally, by using the Einstein relation for long time intervals ($\tau \rightarrow \infty$), the diffusion coefficient parallel to an interface D_i^{xy} can be calculated

$$D_i^{xy}(\mathbf{R}_k) = \frac{\langle \Delta \mathbf{r}(\tau)^2 \rangle_{\mathbf{R}_k}}{2d\tau P(\tau)} = \frac{\sum_{i \in \mathbf{R}_k} [\mathbf{r}_i(\tau) - \mathbf{r}_i(0)]^2}{2d\tau N(0, \tau)} \tag{5}$$

where the time interval was much lower (10 ns) than that used for the calculations of the total diffusion coefficients and ionic conductivities using eqs 1 and 2. Because of this, the values are expected to be far from quantitative, but their qualitative differences and trends should provide insight into how diffusivity is influenced by distance from the alumina surface. This method was shown to give values for water diffusivity, parallel to the interface that were comparable to 3-d diffusivities in bulk, showing that the method does not bias the results.[109]

The lithium transference describes the amount of the conductivity that is due to lithium ion transport. A higher value is sought, as only lithium is oxidized/reduced at the electrodes. Lithium transference is calculated from the ionic diffusivities

$$\tau_+ = \frac{D_+}{D_+ + D_-} \tag{6}$$

where the positive signs represent lithium in this case and negative represents ClO_4^-.

IV. RESULTS AND DISCUSSION

IV.A. Density Profiles. The specific density was calculated as a function of z-position in the calculations. Figure 3 gives the z-dependent specific density profile of the species investigated in the ACID and BASE systems divided by their average densities in the BULK simulations for the temperatures given. The exception to this is alumina, in which the average bulk density was arbitrarily set to 3. The PEO densities show some oscillation near the surface but level out to a value close to the bulk system relatively fast for all systems and temperatures. In general, the PEO density is slightly higher near both alumina surfaces than in the bulk, which was observed for PEO next to TiO_2 surfaces.[70] The lithium and ClO_4^- densities show greater oscillation, between a factor of 0.5 and 1.5 of the bulk density. Of particular interest is that, for the ACID system at 323 K specifically, there appears to be density oscillations between

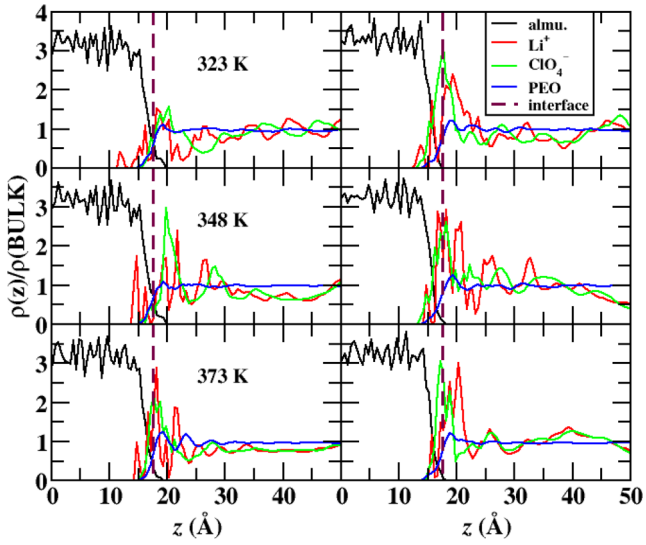

Figure 3. Density profiles divided by their average BULK densities for species investigated with respect to position for the ACID (left) and BASE (right) systems. The alumina density is in arbitrary units.

lithium and ClO_4^- densities that are not as strong in the BASE system. It should be noted that the results at 323 K have 8 times more configurations to determine their properties than at the higher temperatures. In general, the slow movement of the ions still likely requires a further order of magnitude to get very smooth density profiles, but the oscillation for the ACID system was consistent between the different independent simulations. Near the surface, the ion densities are enhanced with respect to the bulk, showing strong interactions between the ions and the surface. The degree of their enhanced density should not be deemed as quantitative, due to their very slow diffusion in this region, which will be discussed later.

IV.B. Conductivities. All temperatures were simulated for a minimum of 200 ns (400 ns at 323 K). For the 348 and 373 K systems, the ionic conductivities and diffusivities of Li^+ and ClO_4^- after 100 ns were found to be similar within their uncertainty of the results at 200 ns. At 323 K, though, the dynamics of the system was so slow that the diffusive region probably is not reached. To get a better gauge of the relationship between diffusion/conductivity and simulation time, we extended the simulations for the 323 K BULK system to 1000 ns. Table 3 gives the conductivities, diffusivities, and lithium transference at different time periods. The errors were extracted from the correlation coefficient from the best fit to the data used to calculate these. It is clear that the conductivities and diffusivities are reduced over time, but the lithium transference appears to be fairly stable over all time periods, changing near its uncertainty limit. This suggests that

Table 3. Conductivities, Diffusivities, and Lithium Transference for Various Simulation Times for the BULK System at 323 K

τ (ns)	$\lambda^{xyz} \times 10^{-4}$ (S/cm)	$D^{xyz}_{Li} \times 10^{-8}$ (cm^2/s)	$D^{xyz}_{ClO_4} \times 10^{-8}$ (cm^2/s)	τ_+
200	0.50 ± 0.06	0.34 ± 0.03	0.87 ± 0.03	0.28 ± 0.03
400	0.36 ± 0.05	0.29 ± 0.02	0.72 ± 0.04	0.29 ± 0.03
600	0.30 ± 0.04	0.24 ± 0.03	0.67 ± 0.06	0.27 ± 0.03
800	0.25 ± 0.04	0.22 ± 0.03	0.64 ± 0.04	0.25 ± 0.03
1000	0.27 ± 0.04	0.18 ± 0.03	0.60 ± 0.05	0.23 ± 0.03

dx.doi.org/10.1021/jp307794r | J. Phys. Chem. B 2012, 116, 14922−14932

qualitative comparisons at the lowest temperatures are possible, but quantitative ones are not.

The conductivities calculated in three dimensions for the BULK system along with sets of experimental data, and the conductivities in the *xy* dimensions (parallel to the surface) for the ACID and BASE systems are given in Table 4. All values in Table 4 are from simulations of 200 ns at 348 and 373 K and 400 ns at 323 K, for a consistent comparison. The errors from the two higher temperatures were estimated from the correlation coefficient of the least-squares fit to the data, and the errors from the lower temperature were extracted from the standard error of the mean from the four independent 400 ns simulations used to calculate these properties. At 323 K, the bulk conductivity is lower than that in ref 111 but similar to that given in ref 31, which vary themselves by around a factor of 2. It should be pointed out that investigating sample history found that conductivity measurements at 323 K immediately after cooling the PEO−$LiClO_4$ sample resulted in higher conductivity than after the systems were held for a long time at room temperature (298 K), allowed to crystallize, and heated to 323 K. Since our simulation results do not show evidence of any partial crystallization (nor regions of expelled $LiClO_4$, as shown in Figure 1), we compare with the "cooling scan" results in ref 31. However, it should be noted that, at this temperature, it is difficult to make quantitative estimations due to the challenge of equilibrating at this temperature. It should be emphasized that we ran four independent simulations at 323 K to test the ability of the simulation protocol to equilibrate these systems, and all four simulations were similar.

Table 4. Comparison of Conductivities from the Systems Simulated with Experiment

	system	323 K	348 K	373 K
$\lambda^{xyz} \times 10^{-4}$ (S/cm)	Expt.[a]	0.79 (320 K)	3.67	6.61
	Expt.[b]	0.40		
	BULK	0.36 ± 0.05	1.89 ± 0.46	6.04 ± 1.45
$\lambda^{xy} \times 10^{-4}$ (S/cm)	ACID	0.32 ± 0.05	1.48 ± 0.01	4.87 ± 2.59
	BASE	0.22 ± 0.05	0.51 ± 0.05	3.52 ± 1.66

[a]Reference 112 for $(EO)_{16}LiClO_4$. [b]Reference 31 for $(EO)_{14}LiClO_4$.

The described issues at 323 K should not be present at the higher temperatures, which are in the liquid region of their phase diagram. At 348 K, the simulation result for conductivity is around half of experiment, while there is good agreement between simulation and experiment at 373 K. The ACID system is fairly close to the result in the BULK system, within the uncertainty at 323 and 373 K, while the BASE system has lower conductivity than the ACID system. Similar results were found experimentally for acid and base treated alumina for $LiCF_3SO_3$.[59] In general, experimental work varies in their analysis of the effect of alumina on ionic conductivity in PEO−$LiClO_4$.[31] Recent work investigated how sample history influenced ionic conductivity for this system. It found that heating and then cooling PEO−$LiClO_4$ with 25% nanoparticles present and an EO:Li ratio of 14:1 resulted in an enhancement in conductivity after the cooling cycle in comparison with a system with no nanoparticles around 323 K.[31] However, the same study found that, before the first and second heating cycles, the presence of nanoparticles resulted in very similar conductivities than systems without throughout the entire temperature range. This is similar to what we found in the results from the MD simulations for the ACID system, which is only slightly lower than the BULK system, and often within the bounds of uncertainty. This slightly lower conductivity is due to ions binding with the surface alumina atoms.

IV.C. Diffusion and Lithium Transference. While ionic conductivity is an important property to assess general ion transport through electrolytes, only lithium can be oxidized/reduced at the electrodes, and lithium diffusivity is of particular importance. The three-dimensional diffusion coefficients for the ionic species in the BULK system along with diffusion parallel to the interface (D^{xy}) are given in Table 5. Additionally, the lithium transference is given in Table 5. These were from 200 ns runs at 348 and 373 K, in which the uncertainty is taken from the error in the linear fit of the mean square displacement, extracted from the correlation coefficient. For the data at 323 K, we had four independent simulations carried out, and the standard error of the mean was calculated. The only comparison with experiment for these numbers is with the lithium transference, in which a similar system as investigated in this work found a value of 0.198 for a filler-free PEO−$LiClO_4$ system with an EO:Li ratio of 10, and a value of 0.246 with 10 wt % alumina nanoparticles added.[19] These were all at 343 K, which is closest to our results at 348 K, in which we get a lithium transference of 0.25, in reasonable agreement considering the slightly different conditions. At 323 K, lithium diffusion is increased with respect to BULK for the ACID system, while the BASE system has lithium diffusivity similar to what is found in the BULK within the uncertainty. The ClO_4^- diffusivity is faster for the ACID system also, while lower in the BASE system than in BULK at 323 K. The lithium transference is also higher for the ACID system than the BULK system at 323 K, and the BASE system is similar as in the BULK. At the higher temperatures, the differences between the ACID and BASE systems are much smaller, and while the diffusivity is slightly higher for the ACID and BASE systems than BULK, the lithium transference is relatively unaffected by the presence of the alumina surfaces. Previous work investigating the role of acidic versus basic treatment of alumina found that lithium transference increased when nanoparticles with acid were embedded in PEO−$LiCF_3SO_3$, while it decreased with respect to having no nanoparticles with alumina nanoparticles treated with base.[59] Our work is consistent with this to a degree at 323

Table 5. Diffusion Coefficients for Lithium and ClO_4^-, along with Lithium Transference for the Systems Investigated

	system	323 K, 400 ns	348 K, 200 ns	373 K, 200 ns
$D^{xyz}_{Li} \times 10^{-8}$	BULK	0.29 ± 0.02	1.24 ± 0.32	1.84 ± 0.15
$D^{xy}_{Li} \times 10^{-8}$ (cm^2/s)	ACID	0.50 ± 0.05	1.66 ± 0.03	2.55 ± 0.53
	BASE	0.26 ± 0.10	1.79 ± 0.58	1.80 ± 0.05
$D^{xyz}_{ClO_4} \times 10^{-8}$	BULK	0.72 ± 0.04	3.70 ± 0.72	9.96 ± 0.36
$D^{xy}_{ClO_4} \times 10^{-8}$ (cm^2/s)	ACID	0.90 ± 0.16	5.45 ± 0.63	11.86 ± 0.14
	BASE	0.62 ± 0.04	5.19 ± 0.68	10.02 ± 0.54
τ_+	Expt[a]		0.198 (343 K)	
	BULK	0.29 ± 0.03	0.23 ± 0.03	0.16 ± 0.02
	ACID	0.36 ± 0.02	0.24 ± 0.02	0.18 ± 0.03
	BASE	0.29 ± 0.05	0.25 ± 0.04	0.15 ± 0.01

[a]Reference 19 for $(EO)_{10}LiClO_4$.

dx.doi.org/10.1021/jp307794r | J. Phys. Chem. B 2012, 116, 14922−14932

K, but the uncertainty in the BASE system does not allow a quantitative assessment of this. There is clearly a different mechanism that is occurring in the ACID and BASE system, with better performance in the ACID system at 323 K.

IV.D. Transport Properties with Respect to the Alumina Surface. For determination of the mechanism of ions in proximity to the alumina surface, D_i^{xy} was calculated for each ion that stayed in a 10 Å slab for 10 ns (see Figure 2). This is not useful for quantitative comparisons, but the qualitative differences between the different surfaces and regions should provide additional insight. Figure 4 gives the logarithm of the

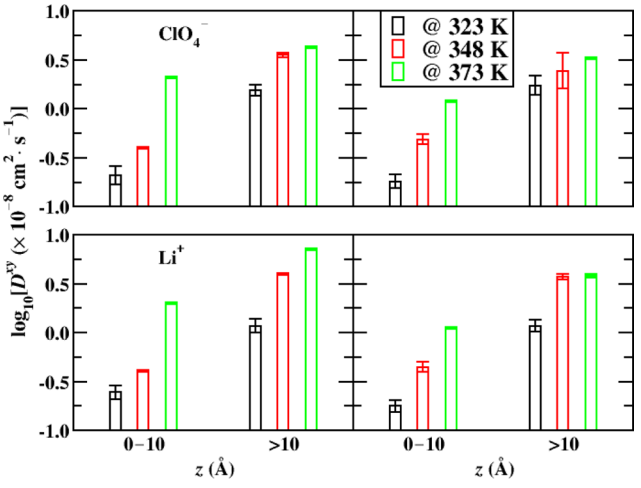

Figure 4. The logarithm for D_i^{xy} for lithium and ClO_4^- ions for the ACID (left) and BASE (right) systems with respect to distance from the alumina surface.

diffusion coefficients parallel to the surface of the ionic species within 10 Å and for regions farther away from alumina surfaces. Next to both alumina surfaces, the diffusion is lower for all species than away from the surface, consistent with previous simulations of ion transport near surfaces.[110] At 323 K, the differences between the ACID and BASE systems are not large enough to be statistically significant, except for lithium diffusion near the alumina surface, which was slightly faster for the ACID system than the BASE system. It is clear that the faster overall diffusivity observed at 323 K is not due to faster diffusion near the surface but faster diffusion away from the surface, even though the PEO densities are nearly identical. It can be observed in the density profile at 323 K (see Figure 3), more so than in the higher temperatures, that there is an oscillation between lithium and ClO_4^- densities, which could promote their dissociation. This will be discussed further in the next section.

The survival probability described in eq 3 can also be used to extract a diffusion coefficient via a dual-simulation procedure with MD paired with Langevin dynamics.[107,108] This could, in principle, be carried out here, but since 10 ns blocks of time were used, the diffusion coefficients extracted would not have much value except for qualitative comparisons. Because of this, the diffusion coefficient was not calculated. Instead, an exponential function of the form $\exp[-(t/\tau_{sur})^{\beta}]$ was fit to the survival probability of lithium and ClO_4^- with respect to time from multiple 10 ns blocks of time extracted from the simulations. The values of β ranged from 0.1 to 0.5 in the fit, while τ_{sur} is a charcteristic time of how long the ions reside in 10 Å regions. In general, the bigger τ_{sur}, the slower the movement of the specific ions, but the described transport is perpendicular to the alumina surface (diffusivities were only for movement parallel to the surface). Figure 5 gives the logarithm

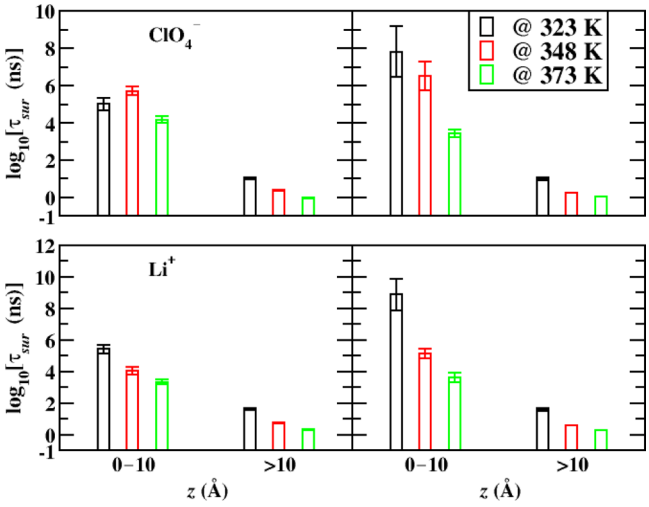

Figure 5. Logarithm of the characteristic time extracted from survival probabilities for lithium and ClO_4^- ions for the ACID (left) and BASE (right) systems with respect to distance from the alumina surface.

of τ_{sur} for different distances from the alumina surface. It can be observed that, for the region closest to the alumina surface, τ_{sur} is significantly higher than the other regions, which away from the surface are on the order of 10 ns and lower. The BASE system has the highest τ_{sur} near the surface, while away from the surface, the ACID and BASE systems show similar results. These results are consistent with the diffusivities estimated for each region.

IV.E. Structural Properties. Radial distribution functions (RDFs) were calculated between a variety of species to investigate the structure of the ACID and BASE systems near and moderately far from the interface. Figure 6 gives the RDFs at 323 K for situations within 10 Å of the alumina surface and when farther away. It is clear that the acidic alumina surface invokes strong structuring between PEO ether oxygens, while this is not observed near the basic surface. Farther away from

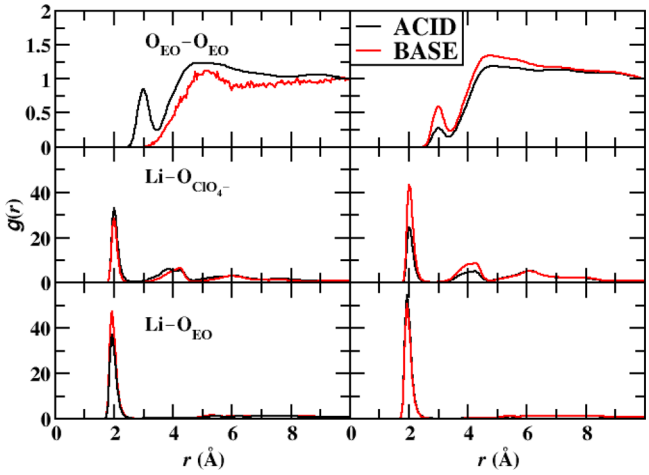

Figure 6. RDFs between species in the regions close to (less than 10 Å, left) and away (greater than 10 Å, right) from the alumina surface at 323 K.

dx.doi.org/10.1021/jp307794r | J. Phys. Chem. B 2012, 116, 14922−14932

the alumina surface, the structuring of ether oxygens is slightly stronger for the BASE system than the ACID system. Stronger EO structuring should, in principle, reduce the amount of lithium binding with EO oxygens. This can be observed in the RDFs, which show that, near the basic surface, lithium−EO binding is stronger than near the acidic surface. The binding between lithium and the anion is similar at both surfaces, but away from the surface, it is weaker for the ACID than BASE system. This result is consistent with the ion density profiles, which show that, at 323 K, lithium and ClO_4^- densities oscillate out of phase for the ACID system but not the BASE system. Figure 7 gives the RDFs between alumina surface oxygens and

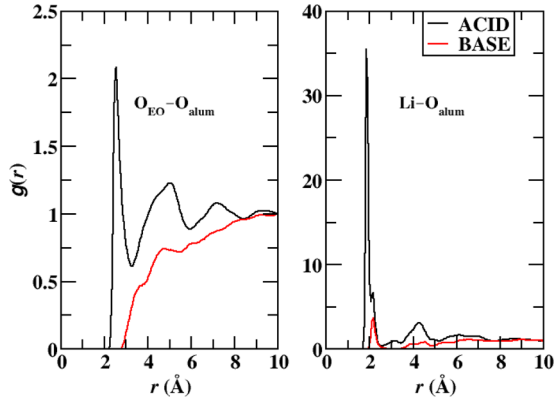

Figure 7. RDF between alumina oxygen with ether oxygens (left) and lithium ions (right) at 323 K.

EO oxygens and lithium ions. There is strong binding between the EO oxygens and the acidic surfaces, which is not present for the BASE system. Lithium ions bind with both surface oxygen groups but much more strongly with the acidic surface. This may seem unexpected, but it should be noted the oxygens are generally strongly bound with two aluminum atoms on the basic surface, versus oxygens on the acidic surface, which are bound with one aluminum atom. Also, lithium binding with acidic oxygens was shown to be stronger than with nonacidic oxygens bound to two aluminum atoms (see Figure 1 and Table 2) from both *ab initio* calculations and the model. This is in contrast to some analysis done previously,[59] in which it was inferred that lithium did not bind strongly with an alumina surface treated with acid. Our findings are in contrast to this, despite giving qualitatively similar results for the effect of acid and base treatment of the alumina surface on ionic conductivity and lithium diffusivity. This shows the need to investigate these effects further to better understand the link between surface interactions and ionic conductivity and diffusivities.

To describe the orientation of the PEO chains, an order parameter was calculated for the PEO chains, in which the average angle between the vectors formed from adjacent PEO oxygens with the z-axis was calculated as a function of position

$$P_2(\cos\theta) = \frac{1}{2}\langle 3\cos^2\theta - 1\rangle \tag{7}$$

where θ is the described angle and the brackets indicate an ensemble average. This function approaches $-1/2$ if the chains are alligned parallel to the surface, 1 if the chains are perpendicular to the surface, and 0 if there is no orientational preference for the PEO chains. P_2 as a function of distance from the interface is given in Figure 8, where zero is an estimate of the surface position. Near the surface, there is strong

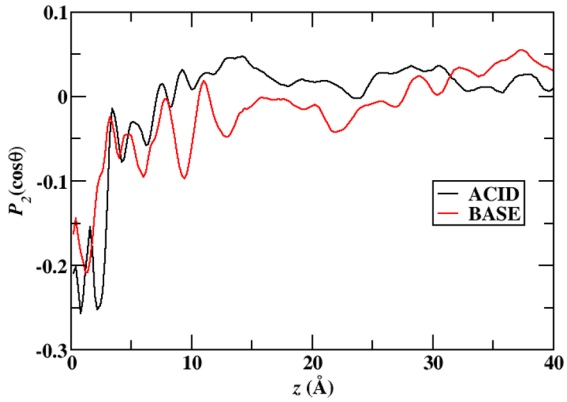

Figure 8. The value of $P_2(\cos\theta)$ as a function of position for PEO at 323 K for the ACID and BASE systems, in which θ is the angle between the vector formed between adjacent PEO oxygens and the z-axis. Zero is an estimate of the alumina surface position.

orientational ordering of the PEO chains, which is present until around 10 Å from the surface. This is similar to other investigations of PEO next to TiO_2 surfaces.[72] Also, there is little difference for PEO ordering between the two surfaces, despite PEO oxygens only strongly binding with the ACID surface. The PEO orientation appears to be based on the available volume instead of the specific surface interactions. There could also be some more subtle differences between the two surfaces that are not being picked up due to the noise in the profile.

IV.F. Lithium Residence Times. The binding of lithium with oxygen molecules was also investigated by calculating the autocorrelation function for binding

$$C_{\mathrm{Li-O}}(t) = \frac{\langle H_{\mathrm{Li-O}}(t) \times H_{\mathrm{Li-O}}(0)\rangle}{\langle H_{\mathrm{Li-O}}(0) \times H_{\mathrm{Li-O}}(0)\rangle} \tag{8}$$

where $H_{\mathrm{Li-O}}(t)$ is an indicator function that is 1 if lithium and a specific oxygen are within 2.5 Å for the entirety of the time interval $(0 - t)$ and zero otherwise. This function is averaged over all potential Li−O pairs, and the value of 2.5 Å was chosen because it represents the first minimum in the Li−O RDF as has been done in previous work.[81] A function that goes exponentially to zero is created, closely following the form $\exp[-(t/\tau_{res})^{\beta}]$, where β and τ_{res} are fit to determine the residence time, τ_{res}. The value of β ranged from 0.3 to 0.6 in the fits, and the results for τ_{res} are listed in Table 6 with the uncertainties calculated from four independent blocks throughout the simulation. There is a clear trend at all temperatures for

Table 6. Mean Residence Time (τ_{res}) for Lithium Binding with EO Oxygens, ClO_4^-, and Alumina Oxygens for All SOLID System Studies at All Temperatures

system	τ_{res} (ns)	323 K	348 K	373 K
BULK	Li−O_{EO}	2.27 ± 0.04	1.27 ± 0.04	0.71 ± 0.10
	Li−O_{ClO_4}	0.13 ± 0.01	0.08 ± 0.01	0.06 ± 0.01
ACID	Li−O_{EO}	2.74 ± 0.26	1.32 ± 0.01	0.80 ± 0.01
	Li−O_{ClO_4}	0.17 ± 0.03	0.10 ± 0.01	0.07 ± 0.01
	Li−O_{alum}	169.24 ± 77.26	31.87 ± 1.31	33.37 ± 3.88
BASE	Li−O_{EO}	3.18 ± 0.12	1.64 ± 0.03	0.88 ± 0.02
	Li−O_{ClO_4}	0.31 ± 0.01	0.21 ± 0.01	0.09 ± 0.01
	Li−O_{alum}	0.05 ± 0.12	0.40 ± 0.03	0.18 ± 0.02

dx.doi.org/10.1021/jp307794r | J. Phys. Chem. B 2012, 116, 14922−14932

the BASE system for lithium to bind longer with the PEO oxygens, and also slightly higher binding with PEO for the ACID system than in the BULK. This trend can also be observed for lithium binding with ClO_4^- oxygens. Binding with the surface alumina is *very* long-lived for the ACID system but rather short for the BASE oxygens, which is consistent with the RDFs in Figure 7. This is likely the reason that there is the strong long-range structure ordering for the ACID system, since lithium ions interacting with the ACID surface reside there for a very long time. The BASE system, on the other hand, does not show such long residence times, and lithium ions are able to bind and unbind to the surface, which should result in less long-range ordering.

To better understand how the surface influences τ_{res}, the analysis was carried out as a function of distance from the alumina surface for the ACID and BASE systems. Figure 9 gives

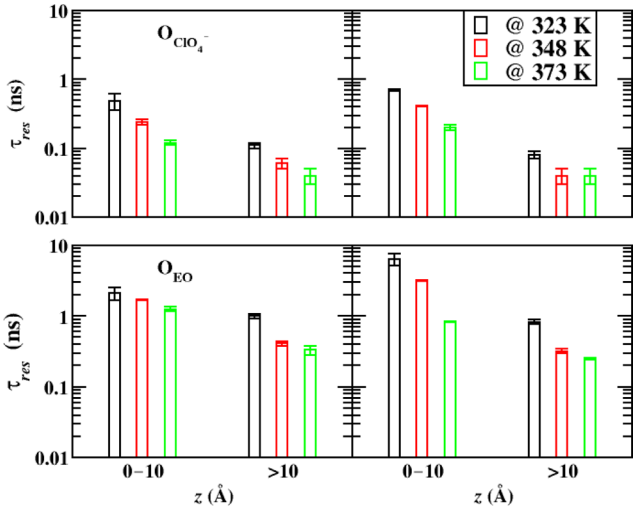

Figure 9. Residence time of lithium binding to ClO_4^- oxygens (top) and PEO oxygens (bottom) for varying distances from the alumina surface for ACID (left column) and BASE (right column) systems at all temperatures investigated.

the τ_{res} for lithium ions near the alumina surface, and away from the surface. The higher lithium residence times are clearly the result of stronger binding near the alumina surfaces for the systems investigated. This is higher for the BASE system than the ACID system, and is present at all temperatures investigated.

V. CONCLUSIONS

Molecular dynamics simulations, aided by Monte Carlo simulations for equilibration, were used to understand how the addition of an acid and base treated alumina surface influences structure, diffusivities, and ionic conductivity for poly(ethylene oxide) with $LiClO_4^-$. The ionic conductivities were not significantly affected by the alumina surfaces, but diffusivities were found to be enhanced at 323 K when acid treated alumina was present. This was linked to long-ranged structural ordering for this temperature of $LiClO_4$, in which the lithium and ClO_4^- densities oscillated out of phase. This was further confirmed with radial distribution functions, which showed weaker binding between lithium and ClO_4^- even significantly away from the acid treated alumina surface. Close to the alumina surface, diffusivity was significantly lower than far away due to higher polymer density and strong binding between the ion and the alumina surface.

AUTHOR INFORMATION

Corresponding Author

*E-mail: cwick@latech.edu.

Notes

The authors declare no competing financial interest.

ACKNOWLEDGMENTS

This research was funded by a grant from the National Science Foundation (NSF EPS-1003897). The calculations were carried out using the resources from the Louisiana Optical Network Initiative (LONI).

REFERENCES

(1) Pinnavaia, T. J.; Beall, G. W. *Polymer-clay nanocomposites*; Wiley: New York, 2002.
(2) Croce, F.; Appetecchi, G. B.; Persi, L.; Scrosati, B. *Nature* **1998**, *394*, 456–458.
(3) Scrosati, B. *Applications of electroactive polymers*; Springer: 1993.
(4) MacCallum, J. R.; Vincent, C. A. *Polymer electrolyte reviews*; Elsevier: London, 1987; Vol. *1*.
(5) MacCallum, J. R.; Vincent, C. A. *Polymer electrolyte reviews*; Elsevier: London, 1989; Vol. *2*.
(6) Tarascon, J. M.; Armand, M. *Nature* **2001**, *414*, 359–367.
(7) Abraham, K. M. *Electrochim. Acta* **1993**, *38*, 1233–1248.
(8) Abraham, K. M.; Jiang, Z. *J. Electrochem. Soc.* **1997**, *144*, L136–L138.
(9) Johansson, P.; Jacobsson, P. *Electrochim. Acta* **2001**, *46*, 1545–1552.
(10) Kelly, I.; Owen, J. R.; Steele, B. C. H. *J. Electroanal. Chem. Interfacial Electrochem.* **1984**, *168*, 467–478.
(11) Kelly, I. E.; Owen, J. R.; Steele, B. C. H. *J. Power Sources* **1985**, *14*, 13–21.
(12) Abraham, K. M.; Jiang, Z.; Carroll, B. *Chem. Mater.* **1997**, *9*, 1978–1988.
(13) Attewell, A. *J. Power Sources* **1989**, *26*, 195–200.
(14) Balakrishnan, P. G.; Ramesh, R.; Kumar, T. P. *J. Power Sources* **2006**, *155*, 401–414.
(15) Holzapfel, M.; Wursig, A.; Scheifele, W.; Vetter, J.; Novak, P. *J. Power Sources* **2007**, *174*, 1156–1160.
(16) Spotnitz, R.; Franklin, J. *J. Power Sources* **2003**, *113*, 81–100.
(17) Gray, F. M. *Solid polymer electrolytes: Fundamentals and technological applications*; Wiley-VCH Press: Cambridge, U.K., 1991.
(18) Gray, F. M. *Polymer electrolytes*; Royal Society of Chemistry: Great Britain, 1997.
(19) Xi, J.; Ma, X.; Cui, M.; Huang, X.; Zheng, Z.; Tang, X. *Chin. Sci. Bull.* **2004**, *49*, 785–789.
(20) Wieczorek, W.; Stevens, J. R.; Florjańzyk, Z. *Solid State Ionics* **1996**, *85*, 67–72.
(21) Wieczorek, W.; Lipka, P.; Żukowska, G.; Wyciślik, H. *J. Phys. Chem. B* **1998**, *102*, 6968–6974.
(22) Weston, J. E.; Steele, B. C. H. *Solid State Ionics* **1982**, *7*, 81–88.
(23) Weston, J. E.; Steele, B. C. H. *Solid State Ionics* **1982**, *7*, 75–79.
(24) Tsuchida, E.; Ohno, H.; Tsunemi, K.; Kobayashi, N. *Solid State Ionics* **1983**, *11*, 227–233.
(25) Tambelli, C. C.; Bloise, A. C.; Rosário, A. V.; Pereira, E. C.; Magon, C. J.; Donoso, J. P. *Electrochim. Acta* **2002**, *47*, 1677–1682.
(26) Shanmukaraj, D.; Wang, G. X.; Murugan, R.; Liu, H. K. *J. Phys. Chem. Solids* **2008**, *69*, 243–248.
(27) Scrosati, B.; Croce, F.; Persi, L. *J. Electrochem. Soc.* **2000**, *147*, 1718–1721.
(28) Qian, X.; Gu, N.; Cheng, Z.; Yang, X.; Wang, E.; Dong, S. *Electrochim. Acta* **2001**, *46*, 1829–1836.
(29) Park, J. W.; Jeong, E. D.; Won, M.-S.; Shim, Y.-B. *J. Power Sources* **2006**, *160*, 674.

(30) Marcinek, M.; Bac, A.; Lipka, P.; Zalewska, A.; Żukowska, G.; Borkowska, R.; Wieczorek, W. *J. Phys. Chem. B* **2000**, *104*, 11088−11093.
(31) Fullerton-Shirey, S. K.; Maranas, J. K. *J. Phys. Chem. C* **2010**, *114*, 9196−9206.
(32) Capiglia, C.; Mustarelli, P.; Quartarone, E.; Tomasi, C.; Magistris, A. *Solid State Ionics* **1999**, *118*, 73−79.
(33) Singh, T. J.; Bhat, S. V. *J. Power Sources* **2004**, *129*, 280−287.
(34) Choi, J.-W.; et al. *Solid State Ionics* **2007**, *178*, 1235−1241.
(35) Cha, E. H.; Macfarlane, D. R.; Forsyth, M.; Lee, C. W. *Electrochim. Acta* **2004**, *50*, 335−338.
(36) Mao, G.; Saboungi, M.-L.; Price, D. L.; Armand, M.; Mezei, F.; Pouget, S. *Macromolecules* **2002**, *35*, 415−419.
(37) Zygadlo-Monikowska, E.; et al. *J. Power Sources* **2007**, *173*, 734−742.
(38) Wang, C.; Liu, Q.; Cao, Q.; Meng, Q.; Yang, L. *Solid State Ionics* **1992**, *53*−*56*, 1106−1110.
(39) Köster, T. K.-J.; Wüllen, L. v. *Solid State Ionics* **2010**, *181*, 489−495.
(40) Johansson, P.; Ratner, M. A.; Shriver, D. F. *J. Phys. Chem. B* **2001**, *105*, 9016−9021.
(41) Bandara, L. R. A. K.; Dissanayake, M. A. K. L.; Mellander, B.-E. *Electrochim. Acta* **1998**, *43*, 1447−1451.
(42) Chintapalli, S.; Frech, R. *Solid State Ionics* **1996**, *86*−*88*, 341−346.
(43) Golodnitsky, D.; Peled, G. A. a. E. *Solid State Ionics* **2002**, *147*, 141−155.
(44) Golodnitsky, D.; Ardel, G.; Strauss, E.; Peled, E.; Lareah, Y.; Rosenberg, Y. *J. Electrochem. Soc.* **1997**, *144*, 3484−3491.
(45) Zhang, S.; Lee, J. Y.; Hong, L. *J. Power Sources* **2004**, *134*, 95−102.
(46) Kumar, B.; Scanlon, L. G. *J. Electroceram.* **2000**, *5*, 127−139.
(47) Kerr, J. B. In *Lithium batteries: science and technology*; Nazri, G., Pistoia, G., Eds.; Kluwer Academic Publishers: Boston, MA, 2004; p 708.
(48) Berthier, C.; Gorecki, W.; Minier, M.; Armand, M. B.; Chabagno, J. M.; Rigaud, P. *Solid State Ionics* **1983**, *11*, 91−95.
(49) Gorecki, W.; Andreani, R.; Berthier, C.; Armand, M.; Mali, M.; Roos, J.; Brinkmann, D. *Solid State Ionics* **1986**, *18*−*19*, 295−299.
(50) Kim, Y.-T.; Smotkin, E. S. *Solid State Ionics* **2002**, *149*, 29−37.
(51) Xu, J. J.; Ye, H. *Electrochem. Commun.* **2005**, *7*, 829−835.
(52) Li, Y. X.; Yerian, J. A.; Khan, S. A.; Fedkiw, P. S. *J. Power Sources* **2006**, *161*, 1288−1296.
(53) Walls, H. J.; Zhou, J.; Yerian, J. A.; Fedkiw, P. S.; Khan, S. A.; Stowe, M. K.; Baker, G. L. *J. Power Sources* **2000**, *89*, 156−162.
(54) Hou, J.; Baker, G. L. *Chem. Mater.* **1998**, *10*, 3311−3318.
(55) Croce, F.; Persi, L.; Ronci, F.; Scrosati, B. *Solid State Ionics* **2000**, *135*, 47−52.
(56) Appetecchi, G. B.; Croce, F.; Persi, L.; Ronci, F.; Scrosati, B. *Electrochim. Acta* **2000**, *45*, 1481−1490.
(57) Croce, F.; Curini, R.; Martinelli, A.; Persi, L.; Ronci, F.; Scrosati, B.; Caminiti, R. *J. Phys. Chem. B* **1999**, *103*, 10632−10638.
(58) Chung, S. H.; Wang, Y.; Persi, L.; Croce, F.; Greenbaum, S. G.; Scrosati, B.; Plichta, E. *J. Power Sources* **2001**, *97*−*98*, 644−648.
(59) Croce, F.; Persi, L.; Scrosati, B.; Serraino-Fiory, F.; Plichta, E.; Hendrickson, M. A. *Electrochim. Acta* **2001**, *46*, 2457−2461.
(60) Krawiec, W.; Scanlon, J., L. G.; Fellner, J. P.; Vaia, R. A.; Vasudevan, S.; Giannelis, E. P. *J. Power Sources* **1995**, *54*, 310−315.
(61) Kumar, B.; Scanlon, L. G. *Solid State Ionics* **1999**, *124*, 239−254.
(62) Wieczorek, W.; Florjanczyk, Z.; Stevens, J. R. *Electrochim. Acta* **1995**, *40*, 2251−2258.
(63) Choi, B.-K.; Kim, Y.-W.; Shin, K.-H. *J. Power Sources* **1997**, *68*, 357−360.
(64) Best, A. S.; Adebahr, J.; Jacobsson, P.; MacFarlane, D. R.; Forsyth, M. *Macromolecules* **2001**, *34*, 4549−4555.
(65) Shin, J.-H.; Alessandrini, F.; Passerini, S. *J. Electrochem. Soc.* **2005**, *152*, A283−A288.
(66) He, Y.; Chen, Z.; Zhang, Z.; Wang, C.; Chen, L. *Chem. J. Chin. Univ.* **1986**, *7*, 187−189.
(67) Lightfoot, P.; Mehta, M. A.; Bruce, P. G. *Science* **1993**, *262*, 883−885.
(68) Kumar, B.; Scanlon, L. G. *J. Power Sources* **1994**, *52*, 261−268.
(69) McBreen, J.; Lee, H. S.; Yang, X. Q.; Sun, X. *J. Power Sources* **2000**, *89*, 163−167.
(70) Borodin, O.; Smith, G. D.; Bandyopadhyaya, R.; Redfern, P.; Curtiss, L. A. *Modell. Simul. Mater. Sci. Eng.* **2004**, *12*, S73−S89.
(71) Barbier, D.; Brown, D.; Grillet, A.-C.; Neyertz, S. *Macromolecules* **2004**, *37*, 4695−4710.
(72) Borodin, O.; Smith, G. D.; Bandyopadhyaya, R.; Byutner, O. *Macromolecules* **2003**, *36*, 7873−7883.
(73) Kasemägi, H.; Klintenberg, M.; Aabloo, A.; Thomas, J. O. *Solid State Ionics* **2002**, *147*, 367−375.
(74) Kasemägi, H.; Klintenberg, M.; Aabloo, A.; Thomas, J. O. *Electrochim. Acta* **2003**, *48*, 2273−2278.
(75) Kasemägi, H.; Aabloo, A.; Klintenberg, M. K.; Thomas, J. O. *Solid State Ionics* **2004**, *168*, 249−254.
(76) Eijck, L. v.; Best, A. S.; Stride, J.; Kearley, G. J. *Chem. Phys.* **2005**, *317*, 282−288.
(77) Smith, J. S.; Borodin, O.; Smith, G. D.; Kober, E. M. *J. Polym. Sci., Part B: Polym. Phys.* **2007**, *45*, 1599−1615.
(78) Wick, C. D.; Theodorou, D. N. *Macromolecules* **2004**, *37*, 7026−7033.
(79) Stubbs, J. M.; Potoff, J. J.; Siepmann, J. I. *J. Phys. Chem. B* **2004**, *108*, 17596−17605.
(80) Chen, B.; Potoff, J. J.; Siepmann, J. I. *J. Phys. Chem. B* **2001**, *105*, 3093−3104.
(81) Wu, H.; Wick, C. D. *Macromolecules* **2010**, *43*, 3502−3510.
(82) Baaden, M.; Berny, F.; Madic, C.; Wipff, G. *J. Phys. Chem. A* **2000**, *104*, 7659−7671.
(83) Mayo, S. L.; Olafson, B. D.; Goddard, W. A., III. *J. Phys. Chem.* **1990**, *94*, 8897−8909.
(84) Gutiérrez, G.; Johansson, B. *Phys. Rev. B* **2002**, *65*, 104202.
(85) Borodin, O.; Smith, G. D. *J. Phys. Chem. B* **2006**, *110*, 6279−6292.
(86) Borodin, O.; Smith, G. D. *J. Phys. Chem. B* **2006**, *110*, 6293−6299.
(87) Borodin, O.; Smith, G. D. *Macromolecules* **2006**, *39*, 1620−1629.
(88) Borodin, O.; Smith, G. D. *J. Phys. Chem. B* **2006**, *110*, 4971−4977.
(89) Borodin, O.; Smith, G. D. *Macromolecules* **2007**, *40*, 1252−1258.
(90) Borodin, O.; Smith, G. D.; Henderson, W. *J. Phys. Chem. B* **2006**, *110*, 16879−16886.
(91) Borodin, O.; Smith, G. D.; Douglas, R. *J. Phys. Chem. B* **2003**, *107*, 6824−6837.
(92) Lascaud, S. University of Montreal, 1996.
(93) Allen, M. P.; Tildesley, D. J. *Computer simulation of liquids*; Oxford University Press: 1987.
(94) Essmann, U.; Perera, L.; Berkowitz, M. L.; Darden, T.; Lee, H.; Pedersen, L. G. *J. Chem. Phys.* **1995**, *103*, 8577−8593.
(95) Mozalev, A.; Magaino, S.; Imai, H. *Electrochim. Acta* **2001**, *46*, 2825−2834.
(96) Berendsen, H. J. C.; Postma, J. P. M.; van Gunsteren, W. F.; DiNola, A.; Haak, J. R. *J. Chem. Phys.* **1984**, *81*, 3684−3690.
(97) Pant, P. V. K.; Theodorou, D. N. *Macromolecules* **1995**, *28*, 7224−7234.
(98) Siepmann, J. I. *Mol. Phys.* **1990**, *70*, 1145−1158.
(99) Siepmann, J. I.; Frenkel, D. *Mol. Phys.* **1992**, *75*, 59.
(100) De Pablo, J. J.; Laso, M.; Suter, U. W. *J. Chem. Phys.* **1992**, *96*, 6157.
(101) Frenkel, D.; Mooij, G. C. A. M.; Smit, B. *J. Phys.: Condens. Matter* **1992**, *4*, 3053.
(102) Wick, C. D.; Siepmann, J. I. *Macromolecules* **2000**, *33*, 7207−7218.
(103) Karayiannis, N. C.; Mavrantzas, V. G.; Theodorou, D. N. *Phys. Rev. Lett.* **2002**, *88*, 105503.
(104) Franks, F.; Mathias, S. F. *Biophysics of water: proceedings of a working conference*; Wiley-Interscience: New York, 1982.

(105) McLaughlin, S. *Annu. Rev. Biophys. Biophys. Chem.* **1989**, *18*, 113−136.
(106) Honig, B. H.; Hubbell, W. L.; Flewelling, R. F. *Annu. Rev. Biophys. Biophys. Chem.* **1986**, *15*, 163−193.
(107) Wick, C. D.; Dang, L. X. *J. Phys. Chem. B* **2005**, *109*, 15574−15579.
(108) Liu, P.; Harder, E.; Berne, B. J. *J. Phys. Chem. B* **2004**, *108*, 6595−6602.
(109) Liu, P.; Harder, E.; Berne, B. J. *J. Phys. Chem. B* **2004**, *108*, 6595−6602.
(110) Borodin, O.; Smith, G. D.; Bandyopadhyaya, R.; Redfern, P.; Curtiss, L. A. *Modell. Simul. Mater. Sci. Eng.* **2004**, *12*, S73−S89.
(111) Sutjianto, A.; Curtiss, L. A. *J. Phys. Chem. A* **1998**, *102*, 968−974.
(112) Choi, B.-K.; Kim, Y.-W. *Electrochim. Acta* **2004**, *49*, 2307−2313.